Dislocations via incompatibilities in phase-field models of microstructure evolution

R. Gröger,[1,*] B. Marchand,[2] and T. Lookman[3]

[1]*CEITEC IPM, Institute of Physics of Materials, Academy of Sciences of the Czech Republic, Žižkova 22, Brno 61600, Czech Republic*

[2]*Université Lille 1, Cité Scientifique, 59655 Villeneuve d'Ascq Cédex, France*

[3]*Los Alamos National Laboratory, Theoretical Division, MS B262, Los Alamos, New Mexico 87545, USA*

(Received 2 September 2015; revised manuscript received 10 June 2016; published 10 August 2016)

We develop a phase-field model that describes the elastic distortion of a ferroelastic material with cubic anisotropy due to an arbitrary dislocation network and a uniform external load. The dislocation network is characterized using the Nye tensor and enters the formulation via a set of incompatibility constraints for the internal strain field. The long-range elastic response of the material is obtained by minimization of the free energy that accounts for higher-order terms of the order parameters and symmetry-adapted strain gradients. The influence of dislocations on the microstructure is studied using a static equilibrium analysis of a material without dislocations and with a random array of parallel edge dislocations. A minimal continuum dislocation dynamics is then used to investigate the simultaneous evolution of the network of geometrically necessary dislocations and the internal strain field. The model developed here is directly applicable to single-phase cubic crystals with an arbitrary degree of anisotropy as well as to ferroelastic materials undergoing temperature-driven cubic-to-tetragonal phase transitions.

DOI: 10.1103/PhysRevB.94.054105

I. INTRODUCTION

The presence of a large density of dislocations in real crystalline materials is often responsible for their complex nonlinear response to external load. Dislocations are metastable defects that move at much lower shear stresses than the theoretical yield strength of the defect-free lattice and are thus dominant carriers of plastic deformation in high-symmetry crystal structures. In martensites, where the phase transition takes place in a coordinated manner without the help of diffusion, dislocations represent preferential sites for heterogeneous nucleation of martensitic embryos [1–4]. These nucleate preferentially in regions of high stress near individual dislocations [5] and grow under the combined effects of temperature, externally applied load [6], image stresses near surfaces [7], or as a result of changes in the dislocation substructure [8,9]. The change of shape of the material that accompanies a martensitic transformation is described by a strain order parameter that may be complemented by other degrees of freedom such as intra-unit-cell displacements (shuffles) or even parameters characterizing local magnetic and electronic ordering in the crystal [10].

The main obstacle in developing continuum models that couple the evolution of dislocation networks with spatially inhomogeneous fields of internal strains and stresses arises from the existence of multiple length scales. The smallest of these corresponds to the Burgers vector of the dislocation, which mostly fits within the range 0.2 to 0.5 nm. Another length scale is that associated with the spacing between dislocations, which is of the order of hundreds of nm depending on the underlying dislocation density. In martensites, there is an additional length scale related to the twin width, W, that ranges from units to hundreds of nm depending on a particular material [11]. The twin width scales as $W \propto |T - T_c|^{-1}$ and thus theoretically diverges at the transition temperature [11,12]. Bridging the length scales in modeling microstructure evolution is clearly a challenging task that may be undertaken by two different approaches. One can utilize a number of different models each representing the behavior of the material within a certain range of scales and requiring that the predictions agree at the interfaces of their domains of applicability. However, a more ambitious project is to develop a single theoretical framework that describes the evolution of microstructure within a wide range of scales from the atomic level up to the continuum.

Phase-field models are among the most widely used techniques for microstructure evolution that are rooted in the use of coarse-grained fields at the mesoscale [13–23]. They are based on the concept of the order parameter [24,25] which was initially developed in the theory of phase transitions to describe symmetry breaking from one structure or phase to another. Khachaturyan and Shatalov [26] extended this idea to model elastic platelet inclusions that are coherent within the surrounding crystal. They showed that the underlying elasticity problem permits a solution for the inhomogeneous strain required to accommodate the platelet inclusions [27]. Hu and Chen [28] used this phase-field microelasticity (PFM) theory in conjunction with the time-dependent Cahn-Hilliard equation to study the evolution of microstructure in anisotropic systems with strong elastic inhomogeneities. The PFM theory was also applied to dislocation loops [17,29–32] which can be viewed as coherent platelet inclusions [33]. Within this theory, dislocations are described by stress-free strains ε^0_{ij} that are nonzero inside dislocation loops and zero outside. This gives rise to the plastic strain tensor, ε^p_{ij}, which represents an incompatible deformation. The same applies to the elastic strain tensor $\varepsilon_{ij} = \varepsilon^t_{ij} - \varepsilon^p_{ij}$ but not to the total strain tensor ε^t_{ij} that is always compatible. The free energy of a deformed material is then written as $F = \int_V (1/2) C_{ijkl} (\varepsilon^t_{ij} - \varepsilon^p_{ij})(\varepsilon^t_{kl} - \varepsilon^p_{kl}) d\boldsymbol{x}$ and minimized with respect to ε^t_{ij} subject to the given field of stress-free (plastic) strains ε^p_{ij}. Adopting the Khachaturyan-Shatalov microelasticity theory, Koslowski

*groger@ipm.cz

et al. [15] developed an incremental variational framework in which the dislocation motion is obtained by a sequence of minimization steps. Kundin *et al.* [34] utilized the PFM theory to obtain the dislocation substructure that is needed to accommodate martensitic needles in the parent austenite matrix. Sreekala and Haataja [35] formulated a phase-field model of dislocation-mediated grain growth in which the driving force is nonlocal due to the long-range strain fields of dislocations. The influence of dislocations on spinodal decomposition was studied by Leonard and Desai [36]. Hunter *et al.* [37] combined the phase-field model of dislocation dynamics with atomistically calculated γ surfaces [38] to study the evolution of dislocation substructures in materials with low and high stacking fault energies. More recently, Levitas and Javanbakht [39–42] developed a phase-field approach for studies of the evolution of dislocations in materials subjected to finite deformations. This model was used to study the ordering of dislocations and their effect on phase stability under high pressures [43].

The objective of the variational models of microstructure evolution is to find the deformation of a body that minimizes the free energy of the system. One way to write this free energy is by using directly the stress-free strains (or eigenstrains) ε^0_{ij} that characterize the dislocation network [44]. The distortion of the body is then obtained by solving numerically the equation of elastodynamics, $\rho\ddot{u}_i = \partial_j\sigma_{ij}$, where ρ is the mass density and u_i the displacement field. The ensuing total strain field ε^t_{ij} is calculated as the gradient of the displacement field and is thus always *compatible* in the sense of the Saint Venant law $\boldsymbol{\nabla}\times\boldsymbol{\nabla}\times\boldsymbol{\varepsilon}^t = \mathbf{0}$. An alternative approach is to write the free energy directly using the *incompatible* elastic strains ε_{ij} and supply additional conditions through which the free energy is informed about the presence of dislocations. These are represented by the set of incompatibility constraints $\boldsymbol{\nabla}\times\boldsymbol{\nabla}\times\boldsymbol{\varepsilon} = \boldsymbol{\eta}$, where η_{ij} is a symmetric tensor field that characterizes the underlying dislocation network. It is defined uniquely by the Nye tensor field [45,46] that describes a spatially continuous distribution of the Burgers vectors of geometrically necessary dislocations (GNDs).

We have demonstrated this formalism previously [47] for edge dislocations in a two-dimensional anisotropic elastic medium of cubic symmetry. The same idea was used in the variational formulation of Groma *et al.* [48], where the Gibbs free energy of a deformed elastic medium is written in terms of internal stresses. In the plane strain case, their model gives predictions that are identical with our strain-based approach. However, the generalization of their model to three dimensions has not been made so far, which is likely due to complications arising from an increase of the number of constraints between the internal fields and the dislocation density. This problem was investigated in our previous publication [49], where we derive a set of three constraint equations that the individual components of the elastic strain tensor have to satisfy in a body with dislocations.

The objective of this paper is to utilize Kröner's continuum theory of dislocations to develop a three-dimensional phase field model in which strain plays the role of the order parameter. An arbitrary dislocation network is described using the Nye tensor that couples to the internal elastic strains through a set of three incompatibility constraints. A notable difference of this method from that of Khachaturyan and Shatalov [15] is that enforcing the constraint of strain compatibility provides analytical expressions for the inhomogeneous strain field that minimizes the free energy without the need for the Green's function of the underlying anisotropic problem. In addition, the presence of symmetry-allowed strain gradients and thus the dispersion character of phonons can be included without much further effort. This will be especially important in capturing the length scale associated with inhomogeneous dislocation substructures [50,51].

This paper is organized as follows. In Sec. II, we outline the essential concepts of a continuum theory of dislocations and develop a method to incorporate an arbitrary dislocation substructure into the field-theoretical description of the free energy of the system. In Sec. III, we perform a careful parametrization of the model to represent Fe-30 at. % Pd, which is a model ferroelastic material exhibiting a temperature-driven martensitic phase transition. In Sec. IV, we investigate the static properties of the model by comparing the internal strain field of a dislocation-free body with a material containing a random array of parallel edge dislocations. In Sec. V, we employ the simplest version of the continuum dislocation dynamics of GNDs to investigate the dynamical properties of the model, in particular the tendency to form correlated dislocation domains above and below the transformation temperature. Section VI summarizes the key elements of our model and its applicability.

II. COUPLING OF DISLOCATIONS WITH INTERNAL STRAINS

A. General formulation

Let us consider a single crystal of cubic symmetry whose bulk is represented by an orthorhombic, fully periodic simulation box discretized by a finite number of cells. The dislocation network will influence the internal strain field only through their geometrically necessary dislocations (GNDs) that represent the combined effect of all crystal dislocations within a cell on its linear-elastic distortion. The density of these GNDs in each cell will be represented by the Nye tensor

$$\alpha_{ij} = \tau_i b_j \rho, \tag{1}$$

where τ_i is the tangential vector (local orientation) of the GND belonging to the given cell, b_j its Burgers vector, and ρ its density. With reference to crystal dislocations, τ_i thus represents the average orientation of a bundle of crystal dislocations [52] embedded in each cell, b_j the Burgers vector of these dislocations, and ρ the number of dislocations piercing the area perpendicular to the dislocation line that corresponds to each cell. Unlike crystal dislocations, GNDs do not have well-defined orientations of their Burgers vectors and, therefore, b_j as well as τ_i and ρ may vary throughout the simulated domain. It is then not surprising that very different dislocation substructures can be described by the same distribution of GNDs and thus the same Nye tensor field. Provided the Nye tensor is known in every cell of the discretized body, it will be possible to obtain the internal strain field by minimizing the free energy of the system. This was previously demonstrated by Groma *et al.* [48] in their two-dimensional variational formulation.

Our objective in the following is to develop a continuum model that describes linear-elastic response of an anisotropic cubic material containing an arbitrary density of GNDs. Under the assumption of small strains, the strain energy density of a deformed anisotropic linear-elastic material is

$$f_{\text{elast}} = \tfrac{1}{2} C_{ijkl}\varepsilon_{ij}\varepsilon_{kl}, \tag{2}$$

where C_{ijkl} is the elastic stiffness tensor, and ε_{ij} the internal elastic strain tensor. To simplify the notation throughout the paper, we employ Einstein summation over repeated indices. There are two sources of internal strain: the externally applied stress Σ_{ij} and the body forces generated by GNDs. The work done by the former per unit volume is

$$f_{\text{load}} = \Sigma_{ij}\varepsilon_{ij}. \tag{3}$$

In order to couple the GNDs with the internal elastic strain ε_{ij}, we will use the incompatibility constraint that was first introduced by Kröner [45]:

$$f_{\text{constr}} = \lambda_{ij}(\epsilon_{ilm}\epsilon_{jpk}\partial_l\partial_p\varepsilon_{km} - \eta_{ij}), \tag{4}$$

where ϵ_{ijk} is the antisymmetric Levi-Civita tensor, η_{ij} the symmetric incompatibility tensor [45,46], and λ_{ij} a symmetric matrix of six Lagrange multipliers. The incompatibility tensor is defined as

$$\eta_{ij} = \tfrac{1}{2}(\epsilon_{ilm}\partial_l\alpha_{jm} + \epsilon_{jlm}\partial_l\alpha_{im}) \tag{5}$$

and relates, through Eq. (4), the nonsymmetric Nye tensor of GNDs, α_{ij}, to the elastic strain tensor ε_{ij}.

The incompatibility tensor vanishes in the body without GNDs. In this case, the displacement field must be single-valued everywhere [53,54], which is true only if the six components of ε_{ij} satisfy six Saint Venant conditions [55–58] that correspond to the vanishing bracket in (4) with $\eta_{ij} = 0$. We have shown previously [49] that three of these equations are the same as the remaining ones and thus only three conditions are needed to ensure that the field ε_{ij} is compatible. If the body contains GNDs, the displacement field is not single-valued across the planar cuts used to create the dislocations. In this case, the incompatibility tensor η_{ij} is no longer zero and (5) represents six nontrivial equations. We have shown in Ref. [49] that only three of these are independent, while the other three are related by the Bianchi identity $\partial_i\alpha_{ij} = 0$, which represents an important condition that dislocations cannot end inside the body [45]. Therefore, if the dislocation network is to be permissible, all dislocations must: (i) form closed loops, or (ii) emanate on the surface of the body. The latter condition is irrelevant here due to the presence of periodic boundary conditions.

The volume integral of the sum of Eqs. (2)–(4) provides the free-energy density of a single-phase material subjected to an arbitrary (but permissible) distribution of GNDs. To broaden the range of applicability of our model, we will further consider that the material can undergo a structural phase transition from the high-symmetry cubic phase into a low-symmetry tetragonal phase, which takes place, for example, in Fe-30 at. % Pd and In-Tl alloys. Following the suggestion of Landau, the free energy of the system must be expanded in powers of a suitably chosen order parameter, keeping only those terms that are invariant with respect to all symmetry operations of the reference structure. This gives rise to the last contribution to the free energy that we denote f_{Landau} and whose explicit form will be given in Sec. II B following the choice of the order parameters.

Up to this point, the elastic strain energy of the deformed body (2) was purely local and thus the model is not able to describe the dispersive character of phonons at larger wave vectors $\boldsymbol{k}$ or phonon softening observed experimentally for materials undergoing structural phase transitions. This missing term can be incorporated by the procedure suggested originally by Ginzburg, i.e., expanding the free energy in terms of the gradients of the order parameters and keeping only those terms that are invariant with respect to all symmetry operations of the reference (cubic) structure. We will return to this in Sec. II B.

By collecting the contributions above, the total free energy of a deformed anisotropic linear-elastic material that undergoes a structural phase transition, contains an arbitrary density of GNDs, and is subjected to external load is written as

$$F = \int_V (f_{\text{elast}} + f_{\text{Landau}} + f_{\text{grad}} - f_{\text{load}} + f_{\text{constr}})\, d\boldsymbol{x}, \tag{6}$$

where the individual contributions to the integrand are given by Eqs. (2)–(4). The explicit forms of the contributions f_{Landau} and f_{grad} are derived in the following subsection.

B. Order parameters and the reduced form of the free energy

Without the loss of generality, we may now simplify the formulation by replacing the six components of the strain tensor ε_{ij} by its cubic eigenstrains e_m ($m = 1,\ldots,6$). These are defined implicitly as

$$\varepsilon_{ij} = \sum_{m=1}^{6} e_m b_{ij}^m, \tag{7}$$

where b_{ij}^m represents six orthonormal basis tensors [59]. Equation (7) can be written explicitly as $\varepsilon_{11} = (1/\sqrt{6})(e_1\sqrt{2} + e_2\sqrt{3} + e_3)$, $\varepsilon_{22} = (1/\sqrt{6})(e_1\sqrt{2} - e_2\sqrt{3} + e_3)$, $\varepsilon_{33} = (1/\sqrt{3})(e_1 - e_3\sqrt{2})$, $\varepsilon_{23} = e_4/\sqrt{2}$, $\varepsilon_{13} = e_5/\sqrt{2}$, and $\varepsilon_{12} = e_6/\sqrt{2}$. The linear relations between the components of ε_{ij} and e_m make it possible to invert these equations to arrive at closed-form expressions of the six deformation parameters: $e_1 = (\varepsilon_{11} + \varepsilon_{22} + \varepsilon_{33})/\sqrt{3}$, $e_2 = (\varepsilon_{11} - \varepsilon_{22})/\sqrt{2}$, $e_3 = (\varepsilon_{11} + \varepsilon_{22} - 2\varepsilon_{33})/\sqrt{6}$, $e_4 = \varepsilon_{23}\sqrt{2}$, $e_5 = \varepsilon_{13}\sqrt{2}$, and $e_6 = \varepsilon_{12}\sqrt{2}$. One immediately sees that, apart from the constant prefactors, e_1 is a measure of the local hydrostatic strain, e_2 and e_3 quantify the local tetragonal deformation, and e_4 to e_6 determine the magnitude of local shear strain. Similarly, we write the applied stress tensor Σ_{ij} in terms of its six cubic eigenstresses S_m, which can be obtained from (7) by the replacements $e_m \to S_m$ and $\varepsilon_{ij} \to \Sigma_{ij}$. The relations between S_m and Σ_{ij} are then identical to those between e_m and ε_{ij}.

Using the substitutions $\varepsilon_{ij} \to e_m$ and $\Sigma_{ij} \to S_m$ defined above, one arrives at equivalent but physically more transparent expressions of the individual components of the free energy. In particular, the strain energy density (2) becomes

$$f_{\text{elast}} = \frac{A_h}{2}e_1^2 + \frac{A_d}{2}\left(e_2^2 + e_3^2\right) + \frac{A_s}{2}\left(e_4^2 + e_5^2 + e_6^2\right), \tag{8}$$

where $A_h = C_{11} + 2C_{12}$, $A_d \equiv C' = C_{11} - C_{12}$, $A_s = 2C_{44}$, and C_{ij} are the three $\langle 100 \rangle$ elastic moduli of a cubic anisotropic material. Similarly, the work done by the applied stress (3) reduces to

$$f_{\text{load}} = S_m e_m \tag{9}$$

and the constraint that couples the density of GNDs with internal elastic strains will be treated in k space as

$$\tilde{f}_{\text{constr}} = \lambda_m \tilde{g}_m, \tag{10}$$

where $m = \{1,2,3\}$ in (9) and (10).

In order to give a particular form of the Landau part of the free energy that depends on higher-order terms of the order parameters, we consider a generic two-phase material that undergoes a cubic-to-tetragonal transition. The free-energy density is assumed to take the form $f = \frac{1}{2} C_{ijkl}\varepsilon_{ij}\varepsilon_{kl} + \frac{1}{3} D_{ijklmn}\varepsilon_{ij}\varepsilon_{kl}\varepsilon_{mn} + \frac{1}{4} E_{ijklmnop}\varepsilon_{ij}\varepsilon_{kl}\varepsilon_{mn}\varepsilon_{op} + \cdots$, where the first term is already represented by f_{elast} above. The irreducible representations of the higher-order terms in this expansion are determined by identifying the components of the tensor D_{ijklmn} that are invariant with respect to the transformations $D_{IJKLMN} = a_{Ii}a_{Jj}a_{Kk}a_{Ll}D_{ijklmn}$, where a_{ij} are transformation matrices representing individual symmetry operations of the parent cubic structure. A similar procedure has to be applied to each tensor in the expansion above. It can be shown that both the third-order and fourth-order terms provide nonvanishing contributions to the free energy. Keeping only the terms that contain the order parameters, we arrive at

$$f_{\text{Landau}} = \frac{B_d}{3} e_3\left(e_3^2 - 3e_2^2\right) + \frac{C_d}{4}\left(e_2^2 + e_3^2\right)^2, \tag{11}$$

where $B_d < 0$ and $C_d > 0$. This expression was given originally by Barsch and Krumhansl [6].

A similar procedure can be used to obtain the gradient part of the free energy, which is written generally as an expansion $f_{\text{grad}} = F_{ijklm}\varepsilon_{ij,m}\varepsilon_{kl} + G^1_{ijklmn}\varepsilon_{ij,mn}\varepsilon_{kl} + G^2_{ijklmn}\varepsilon_{ij,m}\varepsilon_{kl,n} + \cdots$. As shown in Ref. [60], the lowest-order correction vanishes for all centrosymmetric structures, i.e., also for our reference cubic structure. Integrating the second term by parts converts it to the same form as the third term, and thus the lowest order gradient term is $f_{\text{grad}} = G_{ijklmn}\varepsilon_{ij,m}\varepsilon_{kl,n}$. For the cubic symmetry, the tensor G_{ijklmn} contains eleven independent components [61] that are further reduced to two if only the order parameters are considered. In particular, expressing the resultant form of f_{grad} using e_m and keeping only those terms that contain the gradients of the order parameters e_2 and e_3 gives

$$\begin{aligned} f_{\text{grad}} = {} & c_1\left(e_{2,1}^2 + e_{2,2}^2\right) + c_2\left(e_{3,1}^2 + e_{3,2}^2\right) \\ & + c_3(e_{2,1}e_{3,1} - e_{2,2}e_{3,2}) + (4/3)(G_d e_{3,3}^2 + H_d e_{2,3}^2), \end{aligned} \tag{12}$$

where $c_1 = G_d + H_d/3$, $c_2 = G_d/3 + H_d$, and $c_3 = (2/\sqrt{3})(G_d - H_d)$. The above expression thus contains only two independent parameters, G_d and H_d, that can be determined by fitting the curvature of the phonon branch that drives the phase transition. Equation (12) was previously utilized by Rasmussen *et al.* [55] but with only generic coefficients. This expression differs somewhat from the apparently incomplete form given in Ref. [6]. In the case when $G_d = H_d$, as in Ref. [62], the gradient term reduces to $f_{\text{grad}} = (4/3)G_d(|\nabla e_2|^2 + |\nabla e_3|^2)$.

The parameters λ_m in (10) are Lagrange multipliers through which the three incompatibility constraints $g_m = 0$ for $m = \{1,2,3\}$ affect the deformation fields e_m. The k-space representation of these conditions was derived previously in Ref. [49] and we repeat them for convenience:

$$\begin{aligned} \tilde{g}_1 = {} & k_2k_3(\sqrt{2}\tilde{e}_1 + \sqrt{3}\tilde{e}_2 + \tilde{e}_3) \\ & + \sqrt{3}\left(k_1^2\tilde{e}_4 - k_1k_2\tilde{e}_5 - k_1k_3\tilde{e}_6\right) - \sqrt{6}k_2k_3\tilde{N}_1 = 0, \\ \tilde{g}_2 = {} & k_1k_3(\sqrt{2}\tilde{e}_1 - \sqrt{3}\tilde{e}_2 + \tilde{e}_3) \\ & - \sqrt{3}\left(k_1k_2\tilde{e}_4 - k_2^2\tilde{e}_5 + k_2k_3\tilde{e}_6\right) - \sqrt{6}k_1k_3\tilde{N}_2 = 0, \\ \tilde{g}_3 = {} & k_1k_2(\sqrt{2}\tilde{e}_1 - 2\tilde{e}_3) \\ & - \sqrt{3}\left(k_1k_3\tilde{e}_4 + k_2k_3\tilde{e}_5 - k_3^2\tilde{e}_6\right) - \sqrt{6}k_1k_2\tilde{N}_3 = 0. \end{aligned} \tag{13}$$

Given the dislocation substructure and thus both α_{ij} and η_{ij}, the k-space fields $\tilde{N}_1$, $\tilde{N}_2$, and $\tilde{N}_3$ that are needed to implement the three incompatibility constraints (13) are defined as

$$\begin{aligned} \tilde{N}_1 &= \frac{k_1^2\tilde{\eta}_{11} - k_2^2\tilde{\eta}_{22} - k_3^2\tilde{\eta}_{33}}{2k_2^2k_3^2} + \frac{\tilde{\eta}_{23}}{k_2k_3}, \\ \tilde{N}_2 &= \frac{-k_1^2\tilde{\eta}_{11} + k_2^2\tilde{\eta}_{22} - k_3^2\tilde{\eta}_{33}}{2k_1^2k_3^2} + \frac{\tilde{\eta}_{13}}{k_1k_3}, \\ \tilde{N}_3 &= \frac{-k_1^2\tilde{\eta}_{11} - k_2^2\tilde{\eta}_{22} + k_3^2\tilde{\eta}_{33}}{2k_1^2k_2^2} + \frac{\tilde{\eta}_{12}}{k_1k_2}. \end{aligned} \tag{14}$$

One can see from the above that the contributions f_{elast}, f_{Landau}, and f_{load} are all local. However, both f_{grad} and f_{constr} contain gradients of e_m and thus their k-space representations will provide mixing between individual Fourier modes. These terms automatically regularize the deformation field. This regularization must be present in any physically based field-theoretic description of dislocation networks, as previously argued by Groma *et al.* [48].

C. Minimization of the free energy

We now seek the deformation of the body, i.e., the six fields e_m that minimize the free energy (6) with individual terms given by (8)–(12) and the dislocation substructure defined by (14). The conditions of stable equilibrium are $\delta F/\delta e_m = 0$ $(m = 1,\ldots,6)$, $\delta F/\delta\lambda_m = 0$ $(m = 1,2,3)$ and, at the same time, the second derivatives of F with respect to all e_m and λ_m have to be positive. Given the order parameter fields e_2 and e_3, we first find the remaining (non-order-parameter) fields e_1 and e_4 to e_6 that minimize the free energy. The k-space representations of these equilibrium fields are

$$\begin{aligned} \tilde{e}_1 &= \frac{1}{A_h}[S_1\delta(\boldsymbol{k}) - \sqrt{2}(k_2k_3\tilde{\lambda}_1 + k_1k_3\tilde{\lambda}_2 + k_1k_2\tilde{\lambda}_3)], \\ \tilde{e}_4 &= \frac{1}{A_s}[S_4\delta(\boldsymbol{k}) - \sqrt{3}\left(k_1^2\tilde{\lambda}_1 - k_1k_2\tilde{\lambda}_2 - k_1k_3\tilde{\lambda}_3\right)], \end{aligned}$$

$$\tilde{e}_5 = \frac{1}{A_s}[S_5\delta(\boldsymbol{k}) - \sqrt{3}(-k_1k_2\tilde{\lambda}_1 + k_2^2\tilde{\lambda}_2 - k_2k_3\tilde{\lambda}_3)],$$
$$\tilde{e}_6 = \frac{1}{A_s}[S_6\delta(\boldsymbol{k}) - \sqrt{3}(-k_1k_3\tilde{\lambda}_1 - k_2k_3\tilde{\lambda}_2 + k_3^2\tilde{\lambda}_3)]. \quad (15)$$

Substituting these expressions into the three incompatibility constraints (13) yields three algebraic equations for the Fourier images of Lagrange multipliers, $\tilde{\lambda}_m$, as functions of $\tilde{e}_2, \tilde{e}_3$. Substituting these back into (15) provides analytical expressions of the Fourier images of the four non-order-parameter fields in terms of $\tilde{e}_2$ and $\tilde{e}_3$,

$$\tilde{e}_m = \tilde{C}_m^{e_2}\tilde{e}_2 + \tilde{C}_m^{e_3}\tilde{e}_3 + \tilde{C}_m^{\mathrm{rem}}, \quad (16)$$

where $m = \{1,4,5,6\}$, and the kernels $\tilde{C}_m^{e_2}$, $\tilde{C}_m^{e_3}$, $\tilde{C}_m^{\mathrm{rem}}$ are given analytically in Appendices A and B.

The evolution of the two order parameter fields is made using the standard velocity Verlet algorithm,

$$e_i(t+\delta t) = e_i(t) + \dot{e}_i(t)\Delta t - \frac{\delta F(t)}{\delta e_i}\Delta t^2,$$
$$\dot{e}_i(t+\delta t) = \dot{e}_i(t) - \left[\frac{\delta F(t)}{\delta e_i} + \frac{\delta F(t+\Delta t)}{\delta e_i}\right]\Delta t, \quad (17)$$

where $i = \{2,3\}$, and the effective mass was taken as $m = 1/2$. When solving the problem numerically, care must be exercised when calculating the values of certain fields that correspond to zero components of the wave vector $\boldsymbol{k}$. In Appendix B, we identify the sources of these singularities and provide analytical expressions for $\tilde{C}_m^{e_2}$, $\tilde{C}_m^{e_3}$, $\tilde{C}_m^{\mathrm{rem}}$ in (16) for zero components of the wave vector $\boldsymbol{k}$ and their combinations.

In order to simplify the implementation of the model developed in this paper, we summarize below the main steps to calculate the internal stress and strain fields subject to a given distribution of GNDs represented by the Nye tensor α_{ij}.

(1) Determine the Fourier images $\tilde{\alpha}_{ij}$ of the individual components of the Nye tensor. Calculate the k-space components of the incompatibility tensor $\tilde{\eta}_{ij}$ and use them to calculate the three components of the k-space vector $\tilde{N}_i$ defined by (14).

(2) Calculate the k-space fields $\tilde{C}_m^{e_2}$, $\tilde{C}_m^{e_3}$, and $\tilde{C}_m^{\mathrm{rem}}$ for $m = \{1,4,5,6\}$ from Appendices A and B.

(3) Update the two primary fields $\tilde{e}_2$ and $\tilde{e}_3$ according to (17).

(4) Use the two order parameter fields from above in (16) to obtain the remaining fields $\tilde{e}_m$ for $m = \{1,4,5,6\}$.

(5) Fourier-invert the six fields $\tilde{e}_m$ and calculate the real-space representations of the strain field ε_{ij}.

(6) Determine the spatial variation of the individual components of the internal stress tensor as $\sigma_{ij} = \sum_{k=1}^{6}(\delta f^*/\delta e_k)(\partial e_k/\partial \varepsilon_{ij})$, where $f^* = f_{\mathrm{elast}} + f_{\mathrm{Landau}} + f_{\mathrm{grad}}$.

(7) Go back to 3 unless the changes in $\tilde{e}_2$ and $\tilde{e}_3$ are below some specified threshold, i.e., the order parameter fields are not changing any more.

III. PARAMETRIZATION OF THE FREE-ENERGY FUNCTIONAL

In the following simulations, we will consider Fe-30 at. % Pd as a model material that undergoes a temperature-driven martensitic transformation from its high-temperature fcc phase (space group O_h) to the low-temperature fct phase (space group D_{4h}) [63]. The temperature dependencies of the coefficients A_h, A_d, A_s in the harmonic part of the free energy (8) were obtained from the elastic moduli measured by Muto *et al.* [64]. We also make a convenient choice that $G_d = H_d$, which reduces f_{grad} to the form used in Ref. [62]. The numerical value of this coefficient is taken from the same paper.

The coefficients B_d and C_d of the higher-order terms of the free energy (11) were determined as follows. We first identified the extrema of the local part of the free-energy functional that depends on the order parameters:

$$f_{\mathrm{local}} = \frac{A_d}{2}(e_2^2 + e_3^2) + \frac{B_d}{3}e_3(e_3^2 - 3e_2^2) + \frac{C_d}{4}(e_2^2 + e_3^2)^2, \quad (18)$$

where it is customary to express the lowest-order coefficient as $A_d = A_d^0(T - T_0)$ with A_d^0 and T_0 determined by fitting the temperature dependence of the elastic constant C' of the cubic phase. The positions of these extrema are represented by the pairs (e_2^*, e_3^*). One of these is (0,0) which corresponds to the cubic structure. The remaining six roots represent two conjugate sets of tetragonal distortions along the axes x_1, x_2, and x_3. We constructed the Hessian matrix $\boldsymbol{H}$ to find the value(s) of A_d, and thus temperature(s), for which each of these extrema changes character. This occurs when $\det \boldsymbol{H} = 0$ for which the second derivative test is inconclusive, but a small change of A_d (and thus temperature) makes the root a minimum, maximum or a saddle point. For the cubic root at (0,0), this occurs only for $A_d = 0$ (and thus $T = T_0$), where the cubic phase becomes unstable on cooling (this root is a minimum of f_{local} above T_0, and a maximum below T_0). As far as the six remaining roots are concerned, the second derivative test is inconclusive for two values of A_d. One of them is again $A_d = 0$. The other is $A_d = B_d^2/(4C_d)$ that corresponds to the transformation temperature T_c ($> T_0$) at which the tetragonal phase becomes stable on cooling. The two tetragonal roots at $(0, e_3^*)$ are defined by $e_3^* = -(B_d \pm \sqrt{B_d^2 - 4A_dC_d})/(2C_d)$. For $A_d = 0$, i.e., at the temperature T_0, this is $e_3^*(T_0) = -B_d/C_d$. Similarly, for $A_d = B_d^2/(4C_d)$ and thus temperature T_c, we get $e_3^*(T_c) = -B_d/(2C_d)$. These values e_3^* can be obtained from temperature dependencies of the lattice parameters measured by x-ray diffraction [63,65]. In particular, $e_3^*(T_0) = 2(a_t - c_t)/(a_c\sqrt{6})$, where $a_c = 3.75$ Å is the reference lattice parameter of the cubic phase measured at T_c, and $a_t = 3.79$ Å, $c_t = 3.7$ Å are parameters of the tetragonal phase at T_0. The tetragonal distortion at T_0 is then $e_3^* = 0.020$ and thus $B_d = -0.020C_d$. Because the temperature T_c is known from x-ray diffraction measurements [63,65], we can combine this with the equation $A_d(T_c) = B_d^2/(4C_d)$ to obtain both coefficients B_d and C_d. The former is negative and the latter positive as required for the existence of a convex free-energy well.

The summary of all parameters of the free-energy functional used here is given in Table I. The temperature T_0 is obtained directly from the temperature dependence of the elastic moduli measured by Muto *et al.* [64] and agrees well with the maximum temperature for which a diffraction peak

TABLE I. Parameters of the free-energy functional for Fe-30 at. % Pd, where the temperature T is given in Kelvins.

T_0	270	K	
T_c	273	K	
$A_h\ (= C_{11} + 2C_{12})$	$563.0 - 0.536T$	GPa	
$A_d\ (= C' = C_{11} - C_{12})$	$0.460(T - T_0)$	GPa	
$A_s\ (= 2C_{44})$	$143.5 + 0.002T$	GPa	
B_d	-276.0	GPa	
C_d	13800.0	GPa	
a_c	3.75	Å	
ρ	8.91	g/cm^3	Ref. [66]
G_d/a_c^2, H_d/a_c^2	84.0	GPa	Ref. [62,67]

corresponding to the tetragonal lattice parameter a_t is observed in Ref. [65]. Within the narrow range of temperatures $\langle T_0, T_c\rangle$, the tetragonal phase is not yet fully formed and the microstructure is characterized by the so-called pre-transformational tweed [67,68].

In Fig. 1, we show two contour maps of f_{local} calculated at different temperatures using the parameters given in Table I. In particular, Fig. 1(a) corresponds to $T < T_0$, where the white dots in dark areas represent stable tetragonal distortions of the parent cubic structure along the x_1, x_2, and x_3 axes. The remaining three dots in the vicinity of (0,0) represent saddle-points of f_{local} and the dot at (0,0) is the metastable cubic structure. In Fig. 1(b), i.e., at $T > T_c$, there is a single (global) minimum at (0,0) that corresponds to the cubic phase.

Before proceeding further, it is interesting to look at what effect the two nonlocal terms of the free-energy functional, f_{constr} and f_{grad}, have on the patterning in the two order parameter fields e_2 and e_3. For this purpose, we consider a simulation cell with $32 \times 32 \times 32$ mesoscopic cells with lattice parameters $a_{\text{meso}} = \{3.75, 37.5, 375\}$ nm, and two extreme values of the coefficients of the gradient term, $G_d/a_c^2 = H_d/a_c^2 = \{0, 500\}$. We have investigated these effects for the temperature below T_0, where the tetragonal phase is stable.

If the gradient term is ignored, i.e., $G_d = H_d = 0$, the spatial variation of the deformation of the lattice is entirely due to the compatibility of strains that is enforced by f_{constr}. In this

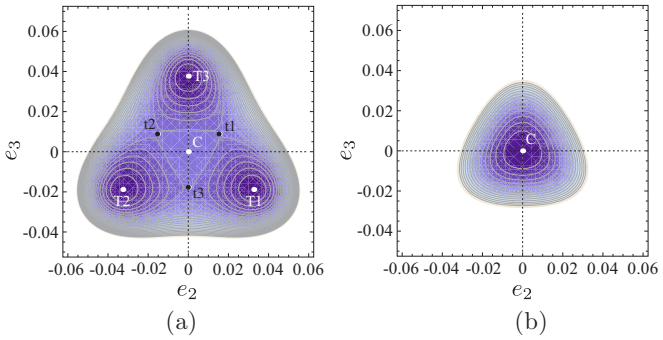

FIG. 1. Contour maps of f_{local} (18) for (a) $T = 250$ K (tetragonal phase stable) and (b) $T = 300$ K (cubic phase stable). The positions of the minima of f_{local} are marked by white dots and the maxima by the black dots. The labels T1–T3 and t1–t3 correspond to tetragonal distortions and C to the undistorted reference cubic lattice.

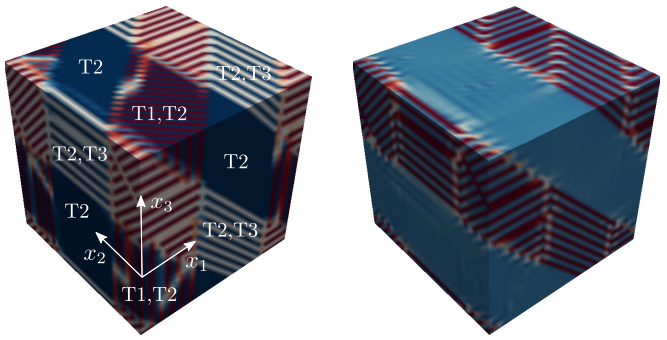

FIG. 2. Order parameter fields (a) e_2 and (b) e_3 calculated for $G_d = H_d = 0$ at the temperature $T = 250$ K, i.e., below T_0. All three tetragonal variants are present in the microstructure. The color range is from -0.03 (darkest blue), via 0 (gray), to 0.03 (darkest red). The labels T1–T3 refer to the minima of f_{local} plotted in Fig. 1(a).

case, the order parameter field e_2 develops the pattern shown in Fig. 2(a) that, together with e_3 [Fig. 2(b)], involves all three variants of the tetragonal phase corresponding to the minima of f_{local} shown in Fig. 1. No change of the microstructure was observed by changing a_{meso} from 3.75 nm to 375 nm. This means that f_{constr} alone does not set the length scale of the problem, as mentioned earlier by Rasmussen *et al.* [55].

When the gradient term is present, the patterning changes substantially. This will be demonstrated in the following by taking extreme values $G_d/a_c^2 = H_d/a_c^2 = 500$ of the coefficient of the gradient term while also keeping the compatibility constraint arising from f_{constr}. If the lattice parameter of the mesoscopic cell is $a_{\text{meso}} = 3.75$ nm, i.e., the edge length of the simulated domain is 0.12 μm, the field e_2 develops a twinned microstructure shown in Fig. 3(a), where the blue and red domains correspond to the two variants of the tetragonal phase shown in Fig. 1 for $e_3 < 0$. If the size of the mesoscopic cell is an order of magnitude larger, i.e., $a_{\text{meso}} = 37.5$ nm (and thus the edge length of the simulated domain is 1.2 μm), the twinned pattern in e_2 still persists [69] as shown in Fig. 3(c). With increasing size of the mesoscopic cell, the gradient term becomes weaker compared to the local terms of the free-energy functional and the microstructure may develop more domain boundaries. This is indeed shown in Fig. 3(e) obtained for $a_{\text{meso}} = 375$ nm (i.e., the edge length of the simulated domain is 12 μm). Here, the fields e_2 and e_3 are similar to those shown in Fig. 2 obtained without the gradient term. This gives rise to fine microstructural details with wavelength comparable to a_{meso}.

IV. MICROSTRUCTURE DUE TO STATIC DISLOCATIONS

In order to illustrate the performance of the model developed in Sec. II, we will first consider a problem of calculating the deformation of Fe-30 at. % Pd mediated by a random array of edge dislocations that are all parallel to the x_3 axis. The simulated block is discretized by a uniform grid of $32 \times 32 \times 32$ mesoscopic cells with edge length $a_{\text{meso}} = 375$ nm, each representing 10^9 underlying atomic-level units

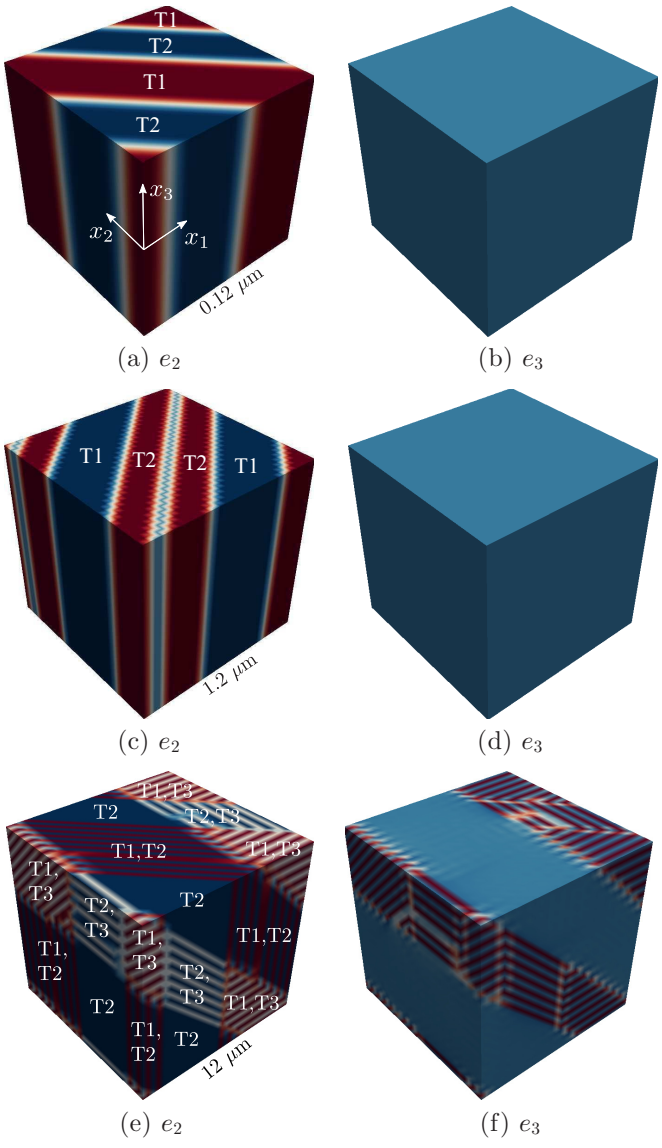

FIG. 3. Influence of the gradient term on the spatial distribution of the order parameter fields e_2 and e_3 for two extreme values of the coefficients G_d and H_d in (12), in particular $G_d/a_c^2 = H_d/a_c^2 =$ 500 GPa, calculated at $T = 250$ K (i.e., below T_0). Three different lattice parameters of the mesoscopic cell were considered here: (a), (b) $a_{\text{meso}} = 3.75$ nm, (c), (d) $a_{\text{meso}} = 37.5$ nm, and (e), (f) $a_{\text{meso}} =$ 375 nm. The color range is from −0.03 (darkest blue), via 0 (gray), to 0.03 (darkest red). The labels T1–T3 refer to the minima of f_{local} plotted in Fig. 1(a).

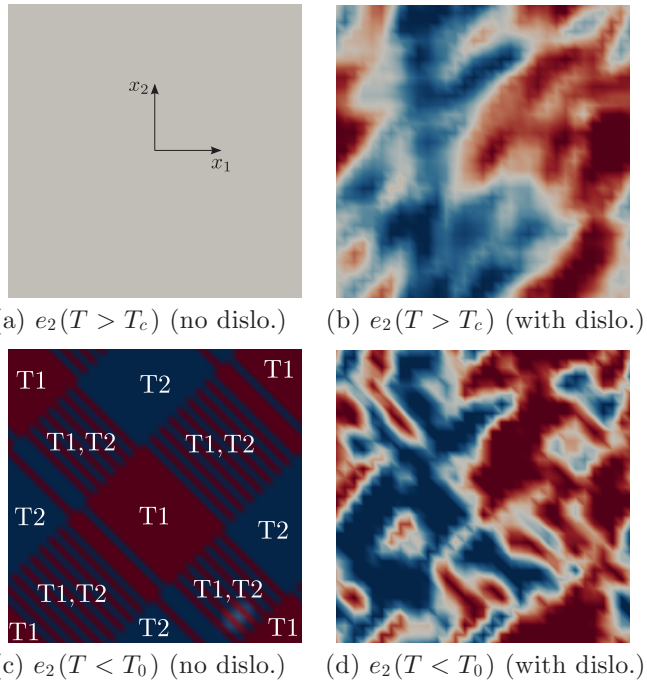

FIG. 4. The partially relaxed order parameter fields e_2 above T_c [(a), (b)] and below T_0 [(c), (d)]. The width (height) of each figure is 12 μm. The panels (a) and (c) correspond to zero dislocation density, whereas in (b) and (d) we consider an array of parallel edge dislocations with line directions perpendicular to the figure. The color range is the same in all figures, from dark blue ($e_2 = -0.03$) via gray ($e_2 = 0$) to dark red ($e_2 = 0.03$).

cells. We consider that all crystal dislocations have Burgers vectors $1/2\langle 110\rangle$ which complies with the fcc structure of the reference cubic phase. No attempt is made here to account for different orientations of the Burgers vectors of dislocations in the tetragonal phase, because we stay within the limits of small-strain elasticity, where also the tetragonal strains (e_2 and e_3) are small. The dislocation network is generated at random using $1/2[110]$ and $1/2[1\bar{1}0]$ edge dislocations with line directions parallel to [001]. Each mesoscopic cell is assigned a random number of 0–100 crystal dislocations with positive and negative Burgers vectors corresponding to $(\bar{1}11)[110]$ and $(111)[1\bar{1}0]$ systems, which results in the dislocation density ρ between 0 and 7.1×10^{14} m^{-2}. The only two nonzero components of the Nye tensor field $\boldsymbol{\alpha}$ are thus α_{31} and α_{32} and their limits are $\pm 1.9 \times 10^{15}$ m^{-1}. We have rescaled these densities to ensure that $\int_V \alpha_{3i} d\boldsymbol{x} = 0$ for $i = 1,2$, which is required in all simulations with periodic boundary conditions to obtain a finite dislocation network.

The order parameter fields e_2 calculated above T_c ($T =$ 300 K) are shown in Figs. 4(a) and 4(b). The former corresponds to zero dislocation density for which the free energy is minimized by an undistorted lattice. Incorporating the array of parallel edge dislocations as explained above results in a nontrivial distribution of deformations in Fig. 4(b) but without patterning. This is obviously expected from the harmonic shape of the free-energy well at this temperature.

The situation is completely different below T_0 ($T = 250$ K) for which the calculated order parameter field develops a noticeable pattern. For zero dislocation density, the partially relaxed field e_2 is shown in Fig. 4(c), whereas that for the dislocation density described above is shown in Fig. 4(d). One can thus see that the twinned microstructure arising due to the presence of the gradient term discussed in the previous section may be strongly modified by dislocations. In particular, the higher the dislocation density the larger the deviation of two order parameter fields e_2 and e_3 from the twinned microstructure.

V. EVOLUTION OF GEOMETRICALLY NECESSARY DISLOCATIONS

Mobile crystal dislocations experience lattice friction stresses and thus their speeds are orders of magnitude lower than vibrational frequencies of the defect-free lattice. This justifies the use of a quasistatic approximation, whereby the dislocation substructure is assumed to be unchanged for a significantly long time so that the internal strain field can come to equilibrium for given boundary conditions and temperature. This minimization is then followed by updating the density of GNDs using the internal stresses obtained from the relaxed fields $e_1 \ldots e_6$. Here, we outline a minimal model of continuum dislocation dynamics that can be used to observe the evolution of GNDs simultaneously with the evolution of internal strain fields. Similar models were developed earlier by Rickman and Viñals [70] and, more recently, by Limkumnerd and Sethna [71], both of which provide evolution laws for the dynamics of plastic strain tensor β_{ij}^p in isotropic media. Adopting the quasistatic approximation above allows us to go beyond these approximations and consider full elastic anisotropy when defining the free energy (6). Moreover, separating the dislocation dynamics from the evolution of the microstructure opens the possibility of introducing atomic-level details into the former. This part is currently a work in progress and will be published separately.

For the total Burgers vector of the GNDs to be conserved during the evolution of the dislocation substructure, the time derivative of the Nye tensor must have the form [72]

$$\dot{\alpha}_{ij} = -\epsilon_{ilm}\partial_l j_{mj}, \tag{19}$$

where $j_{ij} = \epsilon_{ilm}\alpha_{lj}v_m$ represents the dislocation flux density tensor. Combining these two equations and expressing the product of two Levi-Civita tensors using Kronecker delta functions leads to a more transparent form of the above,

$$\dot{\alpha}_{ij} + \partial_l(\alpha_{ij}v_l) = \alpha_{lj}\partial_l v_i. \tag{20}$$

If the right-hand side of this equation were zero, it would represent a continuity equation that describes conservative transport of each component of the Nye tensor separately. The right-hand side of (20) thus represents sources and sinks that are responsible for mixing the individual components of the Nye tensor and thus local rotations and changes of the Burgers vectors and densities of GNDs. The Peach-Koehler force exerted on each dislocation is defined as $F_k = -\epsilon_{ijk}\tau_i\sigma_{jl}b_l$, where σ_{jl} is the internal stress field obtained by the minimization of the free energy in Sec. II. The corresponding dislocation density is obtained as $v_k = \gamma F_k$, where γ is a mobility coefficient.

We have made two dynamical calculations, one above T_c and the other below T_0, to observe the concomitant evolution of the internal microstructure, primarily the order parameter fields e_2 and e_3. All GNDs were initially parallel to the x_3 axis (i.e., the [001] direction), had Burgers vectors parallel to x_1, and their density in the (x_1,x_2) plane was chosen at random such that the magnitude of the total Burgers vector, $B \equiv B_1 = \int_V \alpha_{31} d\boldsymbol{x}$, vanishes. The dislocation density was chosen at random in the range $\rho = \{0, 7.1 \times 10^{12}\}$ m^{-1}. The maximum density is quite small compared to the values typical for metals; it is chosen here for the purpose of highlighting the dislocation—twin boundary interactions without altering significantly the microstructure as shown in Fig. 4. All other

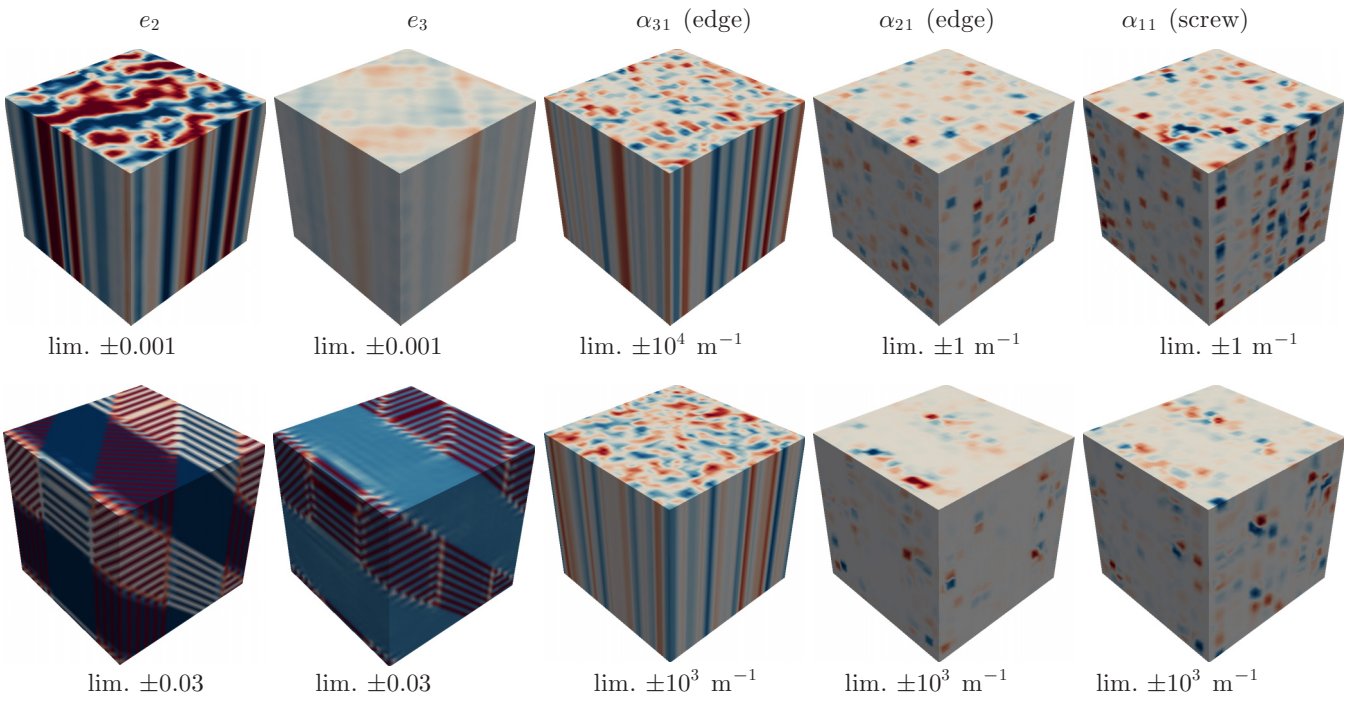

FIG. 5. Order parameter fields e_2 and e_3 and the three nonzero components of the Nye tensor α_{31}, α_{21}, and α_{11} for $T = 300$ K (upper row) and for $T = 250$ K (lower row). The color range is from blue (lowest) via gray (zero) to red (highest) values, whereas the limits corresponding to each color (marked "lim.") are written below each figure.

components of α_{ij} are initially zero. Since the Burgers vector of all GNDs is parallel to x_1, Eq. (20) reduces to a set of three equations,

$$\dot{\alpha}_{i1} + \alpha_{i1}\partial_l v_l = \alpha_{l1}\partial_l v_i \tag{21}$$

where $i = \{1,2,3\}$. Only the glide component of the Peach-Koehler force exerted on the GNDs is used here, which is $F_1^{\text{glide}} = \sigma_{12}b$, and b is the magnitude of the Burgers vector of crystal dislocations. All calculations here were made by applying a small external stress Σ_{12} that makes the GNDs to evolve in the x_1 direction [73]. For the sake of simplicity, Eqs. (21) were integrated using the simple velocity Verlet algorithm with fixed time step. A different approach to integrate these equations that uses the spectral method can be found in the paper of Djaka *et al.* [74].

In Fig. 5, we show the snapshots of the order parameter fields e_2 and e_3 with the corresponding fields α_{31}, α_{21}, and α_{11} obtained by a combination of the continuum dislocation dynamics (21) with the internal stress field obtained from the relaxed fields $e_1 \ldots e_6$. Above T_c (upper row in Fig. 5), both fields e_2 and e_3 are nonzero and nonuniform which is due to finite internal strains contributed by the field of GNDs. The right-hand side of (21) causes the dislocation lines to rotate so that a part of the initially edge-type network of GNDs gives rise to screw GNDs with line directions parallel to x_1 (nonzero α_{11}) and edge dislocations with line directions parallel to x_2 (nonzero α_{21}). This is evident from the nonzero fields α_{21} and α_{11}, respectively.

Below T_0, the fields e_2 and e_3 develop a striped pattern, which resembles that in Fig. 2. The Nye tensor field α_{31} again partially transfers into fields α_{21} and α_{11}. However, the field α_{21} now develops a noticeable pattern whereby larger positive and negative GNDs with line directions parallel to x_2 are concentrated along twin boundaries. Because the glide plane coincides with the (x_1,x_3) plane, these represent localized jogs on the parent edge dislocation that are stabilized by large strain gradients in the vicinity of domain boundaries. The dislocation substructure also builds up nonzero screw components as shown in α_{11}. Our results are in qualitative agreement with experimental observations of defective twinned boundaries in nanotwinned materials [75].

VI. CONCLUSIONS

The field-theoretical model developed in this paper to describe inhomogeneous strain effects combines Kröner's continuum theory of dislocations with the free-energy functional written in terms of the symmetry-adapted components of the elastic strain tensor. The dislocation substructure is described using geometrically necessary dislocations (GNDs) and characterized by the Nye tensor field α_{ij}. The effect of the dislocation network on the internal strain field is described by the symmetric incompatibility tensor η_{ij}, which enters the free-energy functional through a set of three incompatibility constraints imposed using Lagrange multipliers. Dislocations represent a localized source in the incompatibility tensor that also makes the elastic response of the system long-ranged.

The free-energy minimum is sought by first splitting the six components of the internal strain tensor into order-parameter (e_2,e_3) and non-order-parameter (e_1,e_4,e_5,e_6) fields. Using the Euler-Lagrange equations and k-space representations of the three incompatibility constraints, the non-order-parameters are expressed as combinations of two order parameters for a generic material undergoing structural cubic-to-tetragonal phase transitions. Their equilibrium representation is then obtained numerically. The minimization of the free-energy functional in k space necessitates the use of periodic boundary conditions and imposes additional constraints on the character of the dislocation network that can represent a permissible dislocation density.

We demonstrate that the incompatibility of strains arising due to nonzero GNDs frustrates the minimization of the free energy and thus stabilizes the tetragonal deformation for $T > T_c$. Below T_0, the free energy is minimized by developing a twinned microstructure (or a checkerboard pattern) with tetragonal distortions corresponding to the minima of the local part of the free-energy functional. When dislocations are present, they make a preferential choice of the local distortion of the lattice which is spread out through the microstructure due to the existence of long-range cohesive forces.

We further utilize a minimal continuum dislocation dynamics for GNDs to demonstrate the simultaneous evolution of the two order parameter fields and the Nye tensor fields characterizing the density of GNDs. At any temperature, the initial edgelike network of GNDs develops into a complex three-dimensional dislocation substructure in which GNDs locally acquire not only the perpendicular edge but also the screw component. Below T_0, the dislocations develop localized jogs when crossing the twin boundary, which are presumably stabilized by the existence of large deformation gradients in the vicinity of these boundaries.

The variational formulation developed in this paper provides the field of internal elastic stresses and strains corresponding to an arbitrary (but permissible) dislocation network. This model is general for any material of cubic symmetry without or with phase transition between the high-temperature cubic and low-temperature tetragonal phases. The continuum dislocation dynamics used here deals with the evolution of GNDs only, without resolving the contributions from individual slip systems, presence of dislocation sources, dislocation reactions, etc. The latter effects are now being systematically incorporated into the model and will be published separately.

ACKNOWLEDGMENTS

R.G. acknowledges discussions with Giacomo Po on the identification of independent parameters of the strain gradient term. This project was initiated with support by Marie-Curie International Reintegration Grant No. 247705 "MesoPhysDef" and completed as part of Czech Science Foundation Grant No. 16-13797S. Long-term support from the Academy of Sciences of the Czech Republic under Project No. RVO:68081723 is acknowledged. This research was carried out under the project CEITEC 2020 (LQ1601) with financial support from the Ministry of Education, Youth, and Sports of the Czech Republic under the National Sustainability Programme II.

APPENDIX A: ANALYTICAL EXPRESSIONS FOR THE KERNELS $\tilde{C}_m^{e_2}$, $\tilde{C}_m^{e_3}$, AND $\tilde{C}_m^{\mathrm{rem}}$

We have shown in (16) that the fields $\tilde{e}_m$ for $m = \{1,4,5,6\}$ can be obtained at once if the order parameter fields $\tilde{e}_2$ and $\tilde{e}_3$ are known. These expressions involve the kernels $\tilde{C}_m^{e_2}$, $\tilde{C}_m^{e_3}$, and $\tilde{C}_m^{\mathrm{rem}}$ that have to be calculated before minimizing the free energy and then every time the dislocation density or the applied stress changes.

To simplify the expressions, we will make extensive use of the substitutions

$$\begin{aligned} k^2 &= k_1^2 + k_2^2 + k_3^2, \\ d &= 6A_h k_1^2 k_2^2 k_3^2 + A_s\big[k_1^4\big(k_2^2 + k_3^2\big) + k_2^2 k_3^2\big(k_2^2 + k_3^2\big) \\ &\quad + k_1^2\big(k_2^4 + 6k_2^2 k_3^2 + k_3^4\big)\big]. \end{aligned} \tag{A1}$$

Following are the analytical expressions of the k-space kernels $\tilde{C}_m^{e_2}$, $\tilde{C}_m^{e_3}$, and $\tilde{C}_m^{\mathrm{rem}}$ obtained with the help of MATHEMATICA:

$$\begin{aligned} \tilde{C}_1^{e_2} &= \frac{A_s}{d}\sqrt{\frac{3}{2}}\big(k_1^2 - k_2^2\big)k_3^2 k^2, \quad \tilde{C}_1^{e_3} = \frac{A_s}{d\sqrt{2}}\big[k_1^4\big(2k_2^2 - k_3^2\big) - k_2^2 k_3^2\big(k_2^2 + k_3^2\big) + k_1^2\big(2k_2^4 - k_3^4\big)\big], \\ \tilde{C}_1^{\mathrm{rem}} &= \frac{A_s\sqrt{3}}{d}\big[\tilde{N}_1 k_2^2 k_3^2\big(k^2 + k_1^2\big) + \tilde{N}_2 k_1^2 k_3^2\big(k^2 + k_2^2\big) + \tilde{N}_3 k_1^2 k_2^2\big(k^2 + k_3^2\big)\big], \end{aligned} \tag{A2}$$

$$\begin{aligned} \tilde{C}_4^{e_2} &= -\frac{1}{2d}k_2k_3\big\{6A_h k_1^2 k_3^2 + A_s\big[k_2^4 + 3k_2^2k_3^2 + 2k_3^4 + k_1^2\big(k_2^2 + 5k_3^2\big)\big]\big\}, \\ \tilde{C}_4^{e_3} &= -\frac{1}{2d\sqrt{3}}k_2k_3\big\{6A_h k_1^2\big(2k_2^2 - k_3^2\big) + 3A_s\big[k_1^2\big(3k_2^2 - k_3^2\big) + k_2^2\big(k_2^2 + k_3^2\big)\big]\big\}, \\ \tilde{C}_4^{\mathrm{rem}} &= \frac{1}{d\sqrt{2}}k_2k_3\big\{\tilde{N}_1\big[A_s\big(k_2^2 + k_3^2\big)\big(k^2 + k_1^2\big)\big] - \tilde{N}_2\big[6A_h k_1^2 k_3^2 - A_s\big(k_1^2k_2^2 - 3k_1^2k_3^2 - k_2^2k_3^2 - k_3^4\big)\big] \\ &\quad - \tilde{N}_3\big[6A_h k_1^2 k_2^2 + A_s\big(3k_1^2k_2^2 + k_2^4 - k_1^2k_3^2 + k_2^2k_3^2\big)\big]\big\}, \end{aligned} \tag{A3}$$

$$\begin{aligned} \tilde{C}_5^{e_2} &= \frac{1}{2d}k_1k_3\big\{6A_h k_2^2 k_3^2 + A_s\big[k_1^4 + 5k_2^2k_3^2 + 2k_3^4 + k_1^2\big(k_2^2 + 3k_3^2\big)\big]\big\}, \\ \tilde{C}_5^{e_3} &= -\frac{1}{2d\sqrt{3}}k_1k_3\big\{6A_h k_2^2\big(2k_1^2 - k_3^2\big) + 3A_s\big[k_1^4 - k_2^2k_3^2 + k_1^2\big(3k_2^2 + k_3^2\big)\big]\big\}, \\ \tilde{C}_5^{\mathrm{rem}} &= -\frac{1}{d\sqrt{2}}k_1k_3\big(\tilde{N}_1\{6A_h k_2^2 k_3^2 - A_s\big[k_1^2\big(k_2^2 - k_3^2\big) - k_3^2\big(3k_2^2 + k_3^2\big)\big]\big\} \\ &\quad - \tilde{N}_2 A_s\big(k_1^2 + k_3^2\big)\big(k^2 + k_2^2\big) - \tilde{N}_3\big\{6A_h k_1^2 k_2^2 + A_s\big[k_1^4 - k_2^2k_3^2 + k_1^2\big(3k_2^2 + k_3^2\big)\big]\big\}\big), \end{aligned} \tag{A4}$$

$$\begin{aligned} \tilde{C}_6^{e_2} &= -\frac{1}{2d}k_1k_2\big[6A_h\big(k_1^2 - k_2^2\big)k_3^2 + A_s\big(k_1^2 - k_2^2\big)\big(k^2 + 3k_3^2\big)\big], \\ \tilde{C}_6^{e_3} &= \frac{1}{2d\sqrt{3}}k_1k_2\big[6A_h\big(k_1^2 + k_2^2\big)k_3^2 + 3A_s\big(k_1^2 + k_2^2\big)\big(k^2 + k_3^2\big)\big], \\ \tilde{C}_6^{\mathrm{rem}} &= -\frac{1}{d\sqrt{2}}k_1k_2\big(\tilde{N}_1\big\{6A_h k_2^2 k_3^2 + A_s\big[k_2^4 + 3k_2^2k_3^2 + k_1^2\big(k_2^2 - k_3^2\big)\big]\big\} \\ &\quad + \tilde{N}_2\big\{6A_h k_1^2 k_3^2 + A_s\big[k_1^4 - k_2^2k_3^2 + k_1^2\big(k_2^2 + 3k_3^2\big)\big]\big\} - \tilde{N}_3 A_s\big(k_1^2 + k_2^2\big)\big(k^2 + k_3^2\big)\big). \end{aligned} \tag{A5}$$

Because the externally applied load is uniform, it does not appear in the equations above but only in the $\boldsymbol{k} = \boldsymbol{0}$ component of these fields; these are investigated below. Due to the divisions by d, these expressions are only applicable for the wave vectors $\boldsymbol{k} = [k_1k_2k_3]$, where $k_1,k_2,k_3 \neq 0$. The corresponding formulas for the k-space modes with one or more zero components of the wave vector are treated separately in Appendix B.

APPENDIX B: TREATMENT OF ZERO WAVE VECTORS

In order to obtain the expressions for the kernels in (16) when one or more components of the k-space wave vector are zero, one has to begin at the point where the incompatibility constraint is written in terms of the six components of the strain tensor as $\tilde{\boldsymbol{m}}\tilde{\boldsymbol{\varepsilon}} = \tilde{\boldsymbol{\eta}}$. This can be written in the augmented matrix form as [49]

$$\left[\begin{array}{cccccc|c} 0 & -k_3^2 & -k_2^2 & 2k_2k_3 & 0 & 0 & \tilde{\eta}_{11} \\ -k_3^2 & 0 & -k_1^2 & 0 & 2k_1k_3 & 0 & \tilde{\eta}_{22} \\ -k_2^2 & -k_1^2 & 0 & 0 & 0 & 2k_1k_2 & \tilde{\eta}_{33} \\ k_2k_3 & 0 & 0 & k_1^2 & -k_1k_2 & -k_1k_3 & \tilde{\eta}_{23} \\ 0 & k_1k_3 & 0 & -k_1k_2 & k_2^2 & -k_2k_3 & \tilde{\eta}_{13} \\ 0 & 0 & k_1k_2 & -k_1k_3 & -k_2k_3 & k_3^2 & \tilde{\eta}_{12} \end{array}\right], \tag{B1}$$

which is applicable to the wave vectors for which all three components are nonzero. However, care must be exercised when dealing with zero components of the wave vector;

otherwise the solution of the problem will be poisoned with singularities.

1. Wave vector ⟨000⟩

One immediately sees from (B1) that all components of the incompatibility tensor $\tilde{\eta}_{ij}$ must be zero for this wave vector. This was expected because $\boldsymbol{k} = \boldsymbol{0}$ corresponds to a uniform deformation in k space which is automatically compatible. From Eq. (15), it follows at once that

$$\tilde{e}_1 = \frac{1}{A_h} S_1 \delta(\boldsymbol{k}), \qquad \tilde{e}_j = \frac{1}{A_s} S_j \delta(\boldsymbol{k}), \tag{B2}$$

where $j = \{4,5,6\}$. This k-space mode alone thus generates a spatially uniform internal strain field which can be easily incorporated into the model.

2. Wave vectors ⟨k_i00⟩

If two components of the wave vector are zero, whereas the third is nonzero, the system (B1) provides three nontrivial constraints. For example, if $\boldsymbol{k} = [00k_3]$, where $k_3 \neq 0$, the rows 1, 2, 6 of (B1) give the constraints $-k_3^2\tilde{\varepsilon}_{22} = \tilde{\eta}_{11}$, $-k_3^2\tilde{\varepsilon}_{11} = \tilde{\eta}_{22}$, $k_3^2\tilde{\varepsilon}_{12} = \tilde{\eta}_{12}$. The rows 3, 4, 5 reveal that the components of the incompatibility tensor $\tilde{\eta}_{33}$, $\tilde{\eta}_{23}$, $\tilde{\eta}_{13}$ must all vanish for this wave vector and, at the same time, the strain field components $\tilde{\varepsilon}_{33}$, $\tilde{\varepsilon}_{23}$, $\tilde{\varepsilon}_{13}$ can be arbitrary. Similarly, one may obtain the reduced constraints for the wave vectors $\boldsymbol{k} = [0k_20]$ and $\boldsymbol{k} = [k_100]$, where $k_1, k_2 \neq 0$. The minimization of the free energy with respect to the four secondary fields leads to the same form of Eq. (16), where the kernels corresponding to the wave vectors ⟨k_i00⟩ are given in Table II. At the same time, the above-mentioned conditions of vanishing fields $\tilde{\eta}_{33}$, $\tilde{\eta}_{23}$, $\tilde{\eta}_{13}$ for these wave vectors are enforced when constructing the Fourier image of the Nye tensor field.

The variational minimization of the free energy with respect to $\tilde{e}_i$ $(i = 1,4,5,6)$ provides an interesting conclusion that the part of the $\tilde{e}_2$ field for the $\boldsymbol{k} = [00k_3]$ mode cannot be determined independently by (16) but, instead, from

$$\tilde{e}_2 = \frac{1}{\sqrt{2}k_3^2}(\tilde{\eta}_{11} - \tilde{\eta}_{22}). \tag{B3}$$

A similar result is obtained for the other two wave vectors of the ⟨k_i00⟩ group. In particular, the part of the $\tilde{e}_2$ field corresponding to the wave vector $\boldsymbol{k} = [0k_20]$ is defined as

$$\tilde{e}_2 = -\sqrt{3}\tilde{e}_3 + \frac{\sqrt{2}}{k_2^2}(\tilde{\eta}_{11} - \tilde{\eta}_{33}) \tag{B4}$$

and that for the wave vector $\boldsymbol{k} = [k_100]$ is

$$\tilde{e}_2 = \sqrt{3}\tilde{e}_3 + \frac{\sqrt{2}}{k_1^2}(\tilde{\eta}_{33} - \tilde{\eta}_{22}). \tag{B5}$$

These equations are applied after the new field $\tilde{e}_3$ is predicted from (17).

TABLE II. Mathematical expressions of the kernels in (16) for the wave vectors of the type ⟨k_i00⟩.

	$\boldsymbol{k}$		
	$[00k_3]$	$[0k_20]$	$[k_100]$
$\tilde{C}_1^{e_2}$	0	0	0
$\tilde{C}_1^{e_3}$	$-\frac{1}{\sqrt{2}}$	$\sqrt{2}$	$\sqrt{2}$
$\tilde{C}_1^{\text{rem}}$	$-\frac{\sqrt{3}}{2k_3^2}(\tilde{\eta}_{11} + \tilde{\eta}_{22})$	$-\frac{\sqrt{3}}{k_2^2}\tilde{\eta}_{11}$	$-\frac{\sqrt{3}}{k_1^2}\tilde{\eta}_{22}$
$\tilde{C}_4^{e_2}$	0	0	0
$\tilde{C}_4^{e_3}$	0	0	0
$\tilde{C}_4^{\text{rem}}$	0	0	$\frac{\sqrt{2}}{k_1^2}\tilde{\eta}_{23}$
$\tilde{C}_5^{e_2}$	0	0	0
$\tilde{C}_5^{e_3}$	0	0	0
$\tilde{C}_5^{\text{rem}}$	0	$\frac{\sqrt{2}}{k_2^2}\tilde{\eta}_{13}$	0
$\tilde{C}_6^{e_2}$	0	0	0
$\tilde{C}_6^{e_3}$	0	0	0
$\tilde{C}_6^{\text{rem}}$	$\frac{\sqrt{2}}{k_3^2}\tilde{\eta}_{12}$	0	0

3. Wave vectors ⟨k_ik_j0⟩

Let us now assume that only one of the three wave-vector components $\boldsymbol{k}$ is zero, while the remaining two are nonzero. If $\boldsymbol{k} = [0k_2k_3]$, where $k_2, k_3 \neq 0$, the rows 2, 3, 4 of (B1) reduce to $-k_3^2\tilde{\varepsilon}_{11} = \tilde{\eta}_{22}$, $-k_2^2\tilde{\varepsilon}_{11} = \tilde{\eta}_{33}$, and $k_2k_3\tilde{\varepsilon}_{11} = \tilde{\eta}_{23}$. These represent three constraints for the field $\tilde{\varepsilon}_{11}$. Multiplying the row 2 by k_2^2, row 3 by k_3^2, and row 4 by $-k_2k_3$ shows that the left-hand sides of these three equations are identical, while their right-hand sides are different:

$$-k_2^2k_3^2\tilde{\varepsilon}_{11} = k_2^2\tilde{\eta}_{22} = k_3^2\tilde{\eta}_{33} = -k_2k_3\tilde{\eta}_{23}. \tag{B6}$$

In order to satisfy all three conditions, we choose the equation from row 2 as the first constraint that will be imposed when minimizing the free energy. To satisfy the conditions in rows 3 and 4, we must require that $\tilde{\eta}_{33} = (k_2/k_3)^2\tilde{\eta}_{22}$ and $\tilde{\eta}_{23} = -(k_2/k_3)\tilde{\eta}_{22}$, which are both enforced when constructing the incompatibility tensor $\tilde{\eta}_{ij}$ from the given Nye tensor field $\tilde{\alpha}_{ij}$.

Returning back to (B1), the rows 5 and 6 represent two algebraic equations that constrain the internal strain field using the components of the incompatibility tensor $\tilde{\eta}_{13}$ and $\tilde{\eta}_{12}$. Multiplying the row 5 by k_3 and the row 6 by $-k_2$, we find again that the left-hand sides of these equations are identical, while the right-hand sides are different:

$$k_2^2k_3\tilde{\varepsilon}_{13} - k_2k_3^2\tilde{\varepsilon}_{12} = k_3\tilde{\eta}_{13} = -k_2\tilde{\eta}_{12}. \tag{B7}$$

The condition in row 5 is then used as the second constraint that is imposed when minimizing the free energy. The condition in row 6 is satisfied by requiring that $\tilde{\eta}_{12} = -(k_3/k_2)\tilde{\eta}_{13}$ when building the Nye tensor field.

The third constraint is then obtained directly from the row 1 of (B1):

$$-k_3^2\tilde{\varepsilon}_{22} - k_2^2\tilde{\varepsilon}_{33} + 2k_2k_3\tilde{\varepsilon}_{23} = \tilde{\eta}_{11}. \tag{B8}$$

By the procedure above, we have thus obtained the three conditions that constrain the individual components of the internal strain fields, $\tilde{\varepsilon}_{ij}$, for $\boldsymbol{k} = [0k_2k_3]$ subject to a given distribution of dislocations. At the same time, the satisfaction of all six constraints in (B1) yields additional conditions to be satisfied between certain components of the Nye tensor $\tilde{\eta}_{ij}$. Similar results can be obtained for the other two modes

TABLE III. Incompatibility constraints for the wave vectors of the type $\langle k_i k_j 0\rangle$, where $k_i, k_j \neq 0$.

$\boldsymbol{k}$	Constraints
$[0k_2k_3]$	$-k_3^2\tilde{\varepsilon}_{11} = \tilde{\eta}_{22}$
	$k_2^2\tilde{\varepsilon}_{13} - k_2k_3\tilde{\varepsilon}_{12} = \tilde{\eta}_{13}$
	$-k_3^2\tilde{\varepsilon}_{22} - k_2^2\tilde{\varepsilon}_{33} + 2k_2k_3\tilde{\varepsilon}_{23} = \tilde{\eta}_{11}$
	$\tilde{\eta}_{33} = (k_2/k_3)^2\tilde{\eta}_{22}$
	$\tilde{\eta}_{23} = -(k_2/k_3)\tilde{\eta}_{22}$
	$\tilde{\eta}_{12} = -(k_3/k_2)\tilde{\eta}_{13}$
$[k_10k_3]$	$-k_3^2\tilde{\varepsilon}_{22} = \tilde{\eta}_{11}$
	$k_1^2\tilde{\varepsilon}_{23} - k_1k_3\tilde{\varepsilon}_{12} = \tilde{\eta}_{23}$
	$-k_3^2\tilde{\varepsilon}_{11} - k_1^2\tilde{\varepsilon}_{33} + 2k_1k_3\tilde{\varepsilon}_{13} = \tilde{\eta}_{22}$
	$\tilde{\eta}_{33} = (k_1/k_3)^2\tilde{\eta}_{11}$
	$\tilde{\eta}_{13} = -(k_1/k_3)\tilde{\eta}_{11}$
	$\tilde{\eta}_{12} = -(k_3/k_1)\tilde{\eta}_{23}$
$[k_1k_20]$	$-k_2^2\tilde{\varepsilon}_{33} = \tilde{\eta}_{11}$
	$k_1^2\tilde{\varepsilon}_{23} - k_1k_2\tilde{\varepsilon}_{13} = \tilde{\eta}_{23}$
	$-k_2^2\tilde{\varepsilon}_{11} - k_1^2\tilde{\varepsilon}_{22} + 2k_1k_2\tilde{\varepsilon}_{12} = \tilde{\eta}_{33}$
	$\tilde{\eta}_{22} = (k_1/k_2)^2\tilde{\eta}_{11}$
	$\tilde{\eta}_{12} = -(k_1/k_2)\tilde{\eta}_{11}$
	$\tilde{\eta}_{13} = -(k_2/k_1)\tilde{\eta}_{23}$

$[k_10k_3]$ and $[k_1k_20]$ for $k_1,k_2,k_3 \neq 0$. For completeness, we summarize all these constraints in Table III. The expressions of the kernels $\tilde{C}_m^{e_2}$, $\tilde{C}_m^{e_3}$, and $\tilde{C}_m^{\text{rem}}$ for $m = \{1,4,5,6\}$ that are to be used for these modes in (16) are given in Table IV.

TABLE IV. Mathematical expressions of the kernels in (16) for the wave vectors of the type $\langle k_i k_j 0\rangle$, where $k_i, k_j \neq 0$.

	$\boldsymbol{k}$		
	$[0k_2k_3]$	$[k_10k_3]$	$[k_1k_20]$
$\tilde{C}_1^{e_2}$	$-\sqrt{\frac{3}{2}}$	$\sqrt{\frac{3}{2}}$	0
$\tilde{C}_1^{e_3}$	$-\frac{1}{\sqrt{2}}$	$-\frac{1}{\sqrt{2}}$	$\sqrt{2}$
$\tilde{C}_1^{\text{rem}}$	$-\frac{\sqrt{3}}{k_3^2}\tilde{\eta}_{22}$	$-\frac{\sqrt{3}}{k_3^2}\tilde{\eta}_{11}$	$-\frac{\sqrt{3}}{k_2^2}\tilde{\eta}_{11}$
$\tilde{C}_4^{e_2}$	$-\frac{k_2^2+2k_3^2}{2k_2k_3}$	0	0
$\tilde{C}_4^{e_3}$	$-\frac{\sqrt{3}}{2}\frac{k_2}{k_3}$	0	0
$\tilde{C}_4^{\text{rem}}$	$\frac{\tilde{\eta}_{11}k_3^2-\tilde{\eta}_{22}(k_2^2+k_3^2)}{\sqrt{2}k_2k_3^3}$	$\frac{\sqrt{2}}{k_1^2+k_3^2}\tilde{\eta}_{23}$	$\frac{\sqrt{2}}{k_1^2+k_2^2}\tilde{\eta}_{23}$
$\tilde{C}_5^{e_2}$	0	$\frac{k_1^2+2k_3^2}{2k_1k_3}$	0
$\tilde{C}_5^{e_3}$	0	$-\frac{\sqrt{3}}{2}\frac{k_1}{k_3}$	0
$\tilde{C}_5^{\text{rem}}$	$\frac{\sqrt{2}}{k_2^2+k_3^2}\tilde{\eta}_{13}$	$\frac{\tilde{\eta}_{22}k_3^2-\tilde{\eta}_{11}(k_1^2+k_3^2)}{\sqrt{2}k_1k_3^3}$	$-\sqrt{2}\frac{k_2}{k_1(k_1^2+k_2^2)}\tilde{\eta}_{23}$
$\tilde{C}_6^{e_2}$	0	0	$-\frac{k_1^2-k_2^2}{2k_1k_2}$
$\tilde{C}_6^{e_3}$	0	0	$\sqrt{3}\frac{k_1^2+k_2^2}{2k_1k_2}$
$\tilde{C}_6^{\text{rem}}$	$-\sqrt{2}\frac{k_3}{k_2(k_2^2+k_3^2)}\tilde{\eta}_{13}$	$-\sqrt{2}\frac{k_3}{k_1(k_1^2+k_3^2)}\tilde{\eta}_{23}$	$\frac{\tilde{\eta}_{33}k_2^2-\tilde{\eta}_{11}(k_1^2+k_2^2)}{\sqrt{2}k_1k_2^3}$

[1] A. J. Bogers and W. G. Burgers, Acta Metall. **12**, 255 (1964).
[2] G. B. Olson and M. Cohen, J. Less-Common Met. **28**, 107 (1972).
[3] G. B. Olson and A. L. Roitburd, in *Martensite*, edited by G. B. Olson and W. S. Owen (ASM International, Materials Park, OH, 1995), pp. 149–174.
[4] A. C. E. Reid, G. B. Olson, and B. Moran, Phase Trans. **69**, 309 (1999).
[5] L. Kaufman and M. Cohen, Prog. Met. Phys. **7**, 165 (1958).
[6] G. R. Barsch and J. A. Krumhansl, Phys. Rev. Lett. **53**, 1069 (1984).
[7] A. C. E. Reid and G. B. Olson, Mater. Sci. Eng. A **273–275**, 257 (1999).
[8] W. Zhang, Y. M. Jin, and A. G. Khachaturyan, Philos. Mag. **87**, 1545 (2007).
[9] W. Zhang, Y. M. Jin, and A. G. Khachaturyan, Acta Mater. **55**, 565 (2007).
[10] E. K. H. Salje, *Phase Transitions in Ferroelastic and Co-elastic Crystals* (Cambridge University Press, Cambridge, 1993).
[11] J. Chrosch and E. K. H. Salje, J. Appl. Phys. **85**, 722 (1999).
[12] S. A. Hayward, J. Chrosch, E. K. H. Salje, and M. A. Carpenter, Eur. J. Mineral. **8**, 1301 (1996).
[13] Y. M. Jin and A. G. Khachaturyan, Philos. Mag. Lett. **81**, 607 (2001).
[14] L. Q. Chen, Annu. Rev. Mater. Res. **32**, 113 (2002).
[15] M. Koslowski, A. M. Cuitiño, and M. Ortiz, J. Mech. Phys. Sol. **50**, 2597 (2002).
[16] C. Shen and Y. Wang, Acta Mater. **51**, 2595 (2003).
[17] D. Rodney, Y. Le Bouar, and A. Finel, Acta Mater. **51**, 17 (2003).
[18] K. Dayal and K. Bhattacharya, Acta Mater. **55**, 1907 (2007).
[19] V. I. Levitas and D.-W. Lee, Phys. Rev. Lett. **99**, 245701 (2007).
[20] Y. Wang and J. Li, Acta Mater. **58**, 1212 (2010).
[21] V. I. Levitas and M. Javanbakht, Appl. Phys. Lett. **102**, 251904 (2013).
[22] R. Gröger, T. Lookman, and A. Saxena, Phys. Rev. B **78**, 184101 (2008).
[23] J. Kundin, H. Emmerich, and J. Zimmer, Philos. Mag. **91**, 97 (2011).
[24] L. Landau, Nature (London) **138**, 840 (1936).
[25] V. L. Ginzburg, Fiz. Tverd. Tela **11**, 2031 (1960).
[26] A. G. Khachaturyan and G. A. Shatalov, Sov. Phys. JETP **29**, 557 (1969).
[27] A. G. Khachaturyan, S. Semenovskaya, and T. Tsakalakos, Phys. Rev. B **52**, 15909 (1995).
[28] S. Y. Hu and L. Q. Chen, Acta Mater. **49**, 1879 (2001).
[29] Y. U. Wang, Y. M. Jin, A. M. Cuitiño, and A. G. Khachaturyan, Acta Mater. **49**, 1847 (2001).
[30] Y. U. Wang, Y. M. Jin, A. M. Cuitiño, and A. G. Khachaturyan, Appl. Phys. Lett. **78**, 2324 (2001).
[31] Y. U. Wang, Y. M. Jin, and A. G. Khachaturyan, Acta Mater. **51**, 4209 (2003).
[32] D. Rodney and A. Finel, MRS Symp. Proc. **652**, Y4.9.1 (2001).
[33] F. R. N. Nabarro, Proc. Phys. Soc. **59**, 256 (1947).
[34] J. Kundin, D. Raabe, and H. Emmerich, J. Mech. Phys. Solids **59**, 2082 (2011).
[35] S. Sreekala and M. Haataja, Phys. Rev. B **76**, 094109 (2007).
[36] F. Léonard and R. C. Desai, Phys. Rev. B **58**, 8277 (1998).

[37] A. Hunter, I. J. Beyerlein, T. C. Germann, and M. Koslowski, Phys. Rev. B **84**, 144108 (2011).
[38] V. Vitek, Philos. Mag. A **18**, 773 (1968).
[39] V. I. Levitas and M. Javanbakht, Phys. Rev. B **86**, 140101(R) (2012).
[40] V. I. Levitas and M. Javanbakht, J. Mech. Phys. Solids **82**, 345 (2015).
[41] V. I. Levitas and M. Javanbakht, J. Mech. Phys. Solids **82**, 287 (2015).
[42] M. Javanbakht and V. I. Levitas, J. Mech. Phys. Solids **82**, 164 (2015).
[43] V. I. Levitas and M. Javanbakht, Nanoscale **6**, 162 (2014).
[44] The calculations employing finite differences have to use staggered grids, whereby displacements are assigned to the corners and strains to the centroids of cells.
[45] E. Kröner, *Continuum Theory of Dislocations and Self-Stresses* (Springer-Verlag, Berlin, 1958).
[46] E. Kröner, in *Les Houches XXXV - Physics of defects*, edited by R. Balian, M. Kléman, and J. P. Poirier (North-Holland, Amsterdam, 1981), pp. 215–315.
[47] R. Gröger, T. Lookman, and A. Saxena, Philos. Mag. **89**, 1779 (2009).
[48] I. Groma, G. Györgyi, and P. D. Ispánovity, Philos. Mag. **90**, 3679 (2010).
[49] R. Gröger, T. Lookman, and A. Saxena, Phys. Rev. B **82**, 144104 (2010).
[50] H. Mughrabi, T. Ungár, W. Kienle, and M. Wilkens, Philos. Mag. A **53**, 793 (1986).
[51] J. S. Langer, E. Bouchbinder, and T. Lookman, Acta Mater. **58**, 3718 (2010).
[52] This can be shown as follows. Consider N crystal dislocations with the same Burgers vector $\boldsymbol{b}$ that pass through a given cell. The Nye tensor due to the kth such dislocation is then $\alpha_{ij}^k = \tau_i^k b_j \rho^k$, where $\rho^k = l_{\text{dislo}}^k / V_{\text{cell}}$ and l_{dislo}^k is the length of the dislocation segment in the cell of volume V_{cell}. Adopting a simplifying assumption that l_{dislo}^k equals the edge length of the cubic cell, we arrive at $\rho^k \approx 1/S_{\text{cell}}$, where S_{cell} is the area of the cell perpendicular to the dislocation line. The total Nye tensor due to the GNDs in this cell is thus $\alpha_{ij} = \sum_{k=1}^N \alpha_{ij}^k$, which can be expressed in a more transparent way as $\alpha_{ij} = \bar{\tau}_i b_j \bar{\rho}$, which has the same form as that for individual crystal dislocations. Here, $\bar{\tau}_i = (1/N) \sum_{k=1}^N \tau_i^k$ is the average line direction of crystal dislocations passing through the cell, and $\bar{\rho} = N/S_{\text{cell}}$ the density of these dislocations. The GNDs can thus be viewed as "average" dislocations assigned to each cell of the simulated block.
[53] A. P. S. Selvadurai, *Partial Differential Equations in Mechanics*, Vol. 2 (Springer, Berlin, 2000).
[54] L. E. Malvern, *Introduction to the Mechanics of a Continuous Medium* (Prentice-Hall, Englewood Cliffs, NJ, 1969).
[55] K. Ø. Rasmussen, T. Lookman, A. Saxena, A. R. Bishop, R. C. Albers, and S. R. Shenoy, Phys. Rev. Lett. **87**, 055704 (2001).
[56] T. Tran-Cong, Ing. Arch. **55**, 13 (1985).
[57] V. I. Malyi, Prikl. Mat. Mekh. **50**, 679 (1986).
[58] I. V. Andrianov and J. Awrejcewicz, J. Vib. Acoust. **125**, 244 (2003).
[59] M. P. Puls and C. H. Woo, J. Nucl. Mater. **139**, 48 (1986).
[60] D. P. DiVincenzo, Phys. Rev. B **34**, 5450 (1986).
[61] N. Auffray, H. LeQuang, and Q. C. He, J. Mech. Phys. Solids **61**, 1202 (2013).
[62] R. Ahluwalia, T. Lookman, and A. Saxena, Acta Mater. **54**, 2109 (2006).
[63] T. Sohmura, R. Oshima, and F. E. Fujita, Scr. Metall. **14**, 855 (1980).
[64] S. Muto, R. Oshima, and F. E. Fujita, Acta Metall. Mater. **38**, 685 (1990).
[65] H. Seto, Y. Noda, and Y. Yamada, J. Phys. Soc. Jpn. **57**, 3668 (1988).
[66] H. Kato, Y. Liang, and M. Taya, Scr. Mater. **46**, 471 (2002).
[67] R. Oshima, M. Sugiyama, and F. E. Fujita, Metall. Trans. A **19**, 803 (1988).
[68] S. Kartha, J. A. Krumhansl, J. P. Sethna, and L. K. Wickham, Phys. Rev. B **52**, 803 (1995).
[69] The 90° rotation of the two twins relative to those shown in Fig. 3(a) is unimportant because the parent cubic phase is symmetric with respect to 90° rotations.
[70] J. M. Rickman and J. Viñals, Philos. Mag. A **75**, 1251 (1997).
[71] S. Limkumnerd and J. P. Sethna, Phys. Rev. Lett. **96**, 095503 (2006).
[72] L. D. Landau and E. M. Lifshitz, *Theory of Elasticity* (Butterworth-Heinemann, Oxford, 1986), 3rd ed.
[73] Large uniform external load would lead to a single-variant tetragonal phase.
[74] K. S. Djaka, V. Taupin, S. Berbenni, and C. Fressengeas, Model. Simul. Mater. Sci. Eng. **23**, 065008 (2015).
[75] Y. M. Wang, F. Sansoz, T. LaGrange, R. T. Ott, J. Marian, T. W. Barbee, Jr., and A. W. Hamza, Nat. Mater. **12**, 697 (2013).